**MRS Advances © 2016 Materials Research Society**
**DOI: 10.1557/adv.2016.7**

# Comparative study of multilayered nanostructures for enhanced solar optical absorption

Pabitra Dahal[1], Jeffrey Chou[2], Yu Wang[2], Sang Gook Kim[2] and Jaime Viegas[1]

[1]Masdar Institute of Science and Technology, Abu Dhabi, United Arab Emirates

[2] Massachusetts Institute of Technology, Cambridge, Massachusetts, 02139, U.S.A.

## ABSTRACT

Improved solar spectrum optical absorption in multilayered nanostructures consisting of metal, semiconductor and dielectric layers increase their potential for efficient photon to electron conversion. In this work, we analyze the influence of different nanostructure shapes and dimensions on the optical absorption in the vacuum wavelength range of 400 nm to 1500 nm based on Finite Domain Time Difference (FDTD) method. A periodic metallic photonic crystal composed of nanorods of gold, titanium oxide, and alumina is proposed by optimizing thickness of Au and $TiO_2$, aspect ratio, sidewall angle, and geometry of the elemental shape. A high aspect ratio structure consisting of elliptical nose cone elements with optimized dimensions is seen to absorb more than 90% of the solar spectrum in the range considered.

## INTRODUCTION

Better photon to electron conversion is directly related to higher external quantum efficiency, leading to potential applications in photodetectors, photovoltaic and solar water splitting. However, the already limited efficiency of conventional semiconductors like silicon is further restricted by the need to use high bandgap semiconductors such as $TiO_2$ for their chemical robustness in photoelectrochemical solutions.

Different materials have been studied for their photocatalytic activities. The attractiveness of $TiO_2$ in photoelectrochemical process is due to its anti-corrosion and self-cleaning properties [1]. It also has efficient photoactivity, high stability, and lower cost as well as its safeness for human life and environment [2]. According to [3], the morphological states of TiO2 are suitable for both photocatalysis and photocurrent. But, TiO2 can be excited only with ultraviolet light because of its large band gap. Many studies report techniques implemented for extending the photoactivity of $TiO_2$, but they are focused on visible and near infrared region only.

The plasmonic enhancement of optical absorption coupled with hot-carrier injection offers high photon conversion efficiencies with low fabrication costs as compared to conventional electron-hole separation in semiconductor devices [4]. A thin metal layer enhances hot carrier collection, and the mean free path of hot carriers determines the thickness of metal required to avoid their thermalization [5]. Many metals have plasmonic resonance properties that overlap with solar spectrum; however noble metals such as gold are used for their tunable plasmon resonance, high optical cross sections, and stability under harsh chemical conditions [6]. Furthermore, both gold and titanium oxide are been extensively studied materials for water splitting applications. We examine different geometrical combinations of gold and $TiO_2$ in an attempt to arrive to a structure that has strong optical absorption over the whole solar spectrum.

In this work, we will focus on the optical behavior of the layered nanostructures. It is known that carrier transport dynamics are very important for the overall device behavior, especially in a non-planar geometry. This is the focus of future work, as experimental data regarding carrier

recombination and mobility in the thin films needs to be gathered for predictive simulations to be made.

## SIMULATION SETUP

The prototype nanorod structure considered in this work consists of an $Al_2O_3$ nanorod coated with $TiO_2$ and gold layers (figure 1). Silica on top of silicon is used as the platforms for the pillars. The coating of $TiO_2$ and gold is assumed to be conformal, i.e. their thickness on pillars is nearly equal to their thickness on the wafer surface. The non-cylindrical rods are higher degree parabola.

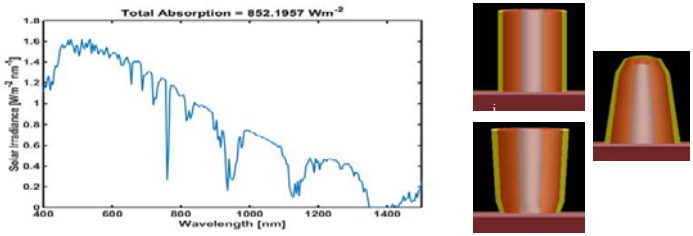


**Figure 1.** (Left) Solar spectrum used to estimate the maximum amount of light that can be absorbed using different variations of nanorods. (Right) nanorods (not in scale) used in simulation: cylindrical, convex nose cone and concave nose cone.

Three dimensional FDTD simulations are performed using commercial software (Lumerical FDTD Solutions). All material properties are obtained from the software's library, and plane wave light excitation is assumed in all work.

To calculate the amount of solar light absorbed by the simulated structure, ASTM G173-03 Reference Spectra [6] corresponding to spectral radiation from solar disk and sky diffuse and diffuse reflected from ground on south facing surface tilted $37^o$ from horizontal is used. The solar spectrum is scaled according to the relative absorption in the wavelength range of 400 nm to 1500 nm and integrated to get the total absorbed power per unit area. Even though our plane wave source is not the most accurate description of realistic solar condition radiation, in terms of angular irradiance distribution, we are mainly interested in the relative performance of the different geometric nanoscale configurations.

We assume periodic boundary conditions on the side boundaries of our unit cell, with each unit cell containing a nanorod. Perfectly matched layers are implemented on the top and bottom boundaries. A plane wave source is defined at the top interface and power monitors are located on planes above and below the nanorods.

Since we perform full wave 3D simulations based on directly discretized Maxwell's equations, the light scattering and trapping behavior is fully taken into account. By using period boundary conditions on the lateral sides of the unit cell, we have taken into account scattering from the nanostructured surface.

## EVALUATION OF DESIGN PARAMETERS

The period of the unit cell is made fairly large while optimizing the thickness of layers so that the change in fill factor during optimization runs does not contribute much to the results. The effect of variation in fill factor is also simulated. Most of the simulation results are based on the concave nose cone nanorods, as these have shown to have higher optical absorption than the two other models in figure 1.

### Semiconductor Thickness

The optical response of nanorods with different thickness of the $TiO_2$ layer as a varying design parameter is simulated with 10 nm of gold layer on an $Al_2O_3$ rod that has 50 nm base diameter. The period of the structure is taken to be 300 nm. With increased thickness of $TiO_2$, the absorption peak moves towards the infrared region (figure 2). Increased infrared absorption is also observed. But above 50 nm thickness, the peak starts to decrease gradually, impacting infrared absorption significantly. The change in peak location and their magnitude is related to the cavity, waveguide, and surface plasmon polariton (SPP) modes and their strength around the respective wavelength. $TiO_2$ thickness of around 40 nm shows higher solar-spectrum integrated absorption.

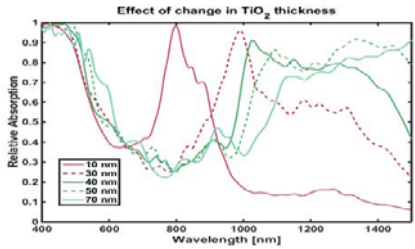


| $TiO_2$ Thickness (nm) | Total Absorption ($Wm^{-2}$) |
|---|---|
| 10 | 461 |
| 20 | 476 |
| 30 | 498 |
| 40 | 511 |
| 50 | 511 |
| 60 | 505 |
| 70 | 498 |
| 80 | 498 |

**Figure 2.** Relative absorption from the nanorod for different thickness of $TiO_2$ layer (left), and total absorption of the solar spectrum over the wavelength range of 400 nm to 1500 nm (right).

### Metal Thickness

With 40 nm of $TiO_2$ layer around $Al_2O_3$ rod, the total absorption is calculated by varying the thickness of the gold layer. The period of the structure is 300 nm. The absorption peaks in the infrared move towards the visible range with an increase in thickness, but they become narrower as well (figure 3). Based on the area of overlap of the relative absorption and solar irradiance graphs, the optimal gold thickness is considered to be 12 nm.

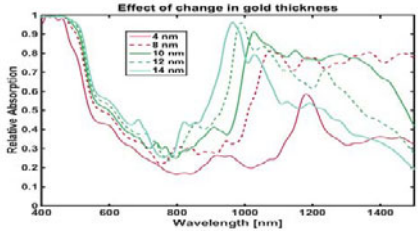


| Gold Thickness | Total Absorption ($Wm^{-2}$) |
|---|---|
| 2 | 320 |
| 4 | 367 |
| 6 | 424 |
| 8 | 475 |
| 10 | 511 |
| 12 | 523 |
| 14 | 522 |
| 16 | 521 |

**Figure 3.** Relative absorption from the nanorod for different thickness of gold layer (left), and total absorption of the solar spectrum over the wavelength range of 400 nm to 1500 nm (right).

**Nanorod height**

For the purpose of determining how the height of the rods change the absorption spectrum, we have simulated the optical properties of $Al_2O_3$ rods with 40 nm of $TiO_2$ and 12 nm of gold coating for different heights of the structure. The structure is periodic in both directions with periodicity of 300 nm. The observed increase of absorption with rod height is primarily due to the increased area for photon-metal interaction (figure 4).

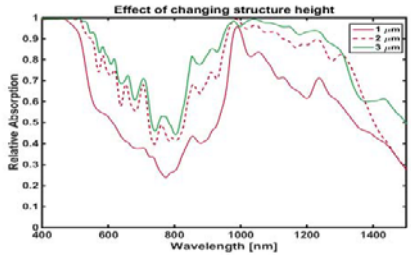


| Structure height (nm) | Total Absorption ($Wm^{-2}$) |
|---|---|
| 500 | 401 |
| 1000 | 523 |
| 1500 | 622 |
| 2000 | 657 |
| 2500 | 681 |
| 3000 | 700 |

**Figure 4.** Relative absorption for a periodic array of nanorods with different rod heights (left), and total absorption of the solar spectrum over the wavelength range of 400 nm to 1500 nm (right).

**Periodicity or fill factor**

The nanorod structure of 50 nm $Al_2O_3$, 40 nm $TiO_2$, 12 nm gold and 1μm height is simulated for different periods to determine how the fill factor changes the absorptive behavior. Denser designs clearly improve the performance (figure 5), due to the larger effective absorption effective area, although fabrication constraints may limit how densely the nanorods can be placed.

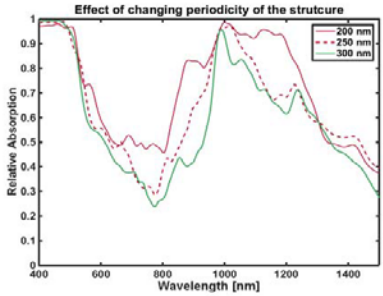


| Nanorod periodicity (nm) | Total Absorption ($Wm^{-2}$) |
|---|---|
| 200 | 628 |
| 250 | 563 |
| 300 | 523 |

**Figure 5.** Relative absorption from the nanorod for different periodicity (left), and total absorption of the solar spectrum over the wavelength range of 400 nm to 1500 nm (right).

## Nanorod geometry

The shape of the rods changes the performance of the device to some extent. The concave nose cone (or nose cone inverted) has a slightly larger overall absorption than the other geometries (figure 6). These types of pillars can interact directly with vertically incident photons.

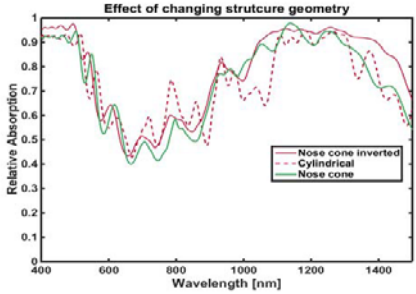


| Unit cell geometry | Total Absorption ($Wm^{-2}$) |
|---|---|
| Nose cone inverted | 620 |
| Nose cone | 596 |
| Cylindrical | 604 |

**Figure 6.** Relative absorption from the nanorod for different rod shapes (left), and total absorption of the solar spectrum over the wavelength range of 400 nm to 1500 nm (right). All pillars have 1 μm height with $Al_2O_3$ base diameter of 50 nm, 50 nm coating of $TiO_2$, and 10 nm coating of gold.

We have combined all the optimal parameters of this study into an optimized structure achieving an estimated 90% absorption efficiency over the full spectral range of interest (400-1500 nm), as observed in figure 7.

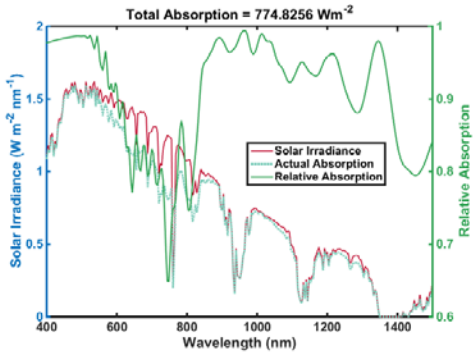


**Figure 7.** Relative absorption spectrum of the optimized device (gree solid line), and comparison of available (red solid line) and absorbed (dotted blue line) solar radiation. The inverted nose cone nanorod with 50 nm $Al_2O_3$, 40 nm $TiO_2$, 12 nm gold, 3 μm height and 200 nm periodicity is simulated from the optimization reported in this work.

## CONCLUSIONS

The optimized thickness of gold and $TiO_2$ increase the photon metal interaction in the structure and shift the resonant mode frequencies. The adjustment in height, shape, and periodicity ensures maximum amount of light absorption at the device. Fine tuning of all these parameters aids to enhance solar absorption. Through simulation, a $TiO_2$ layer of thickness 40 nm and gold layer of thickness 12 nm around 50 nm thick $Al_2O_3$ rod is determined to be one of the optimal designs. Higher aspect ratio structures and densely placed structures show higher absorption, but may not be feasible due to fabrication constraints. Nevertheless, these optimizations give promising results with easily achievable fabrication aspect ratios and surface structure density. An estimated 90% absorption efficiency over a broad solar spectral range (400-1500 nm) is achieved with an optimized structure as presented in this work.

## ACKNOWLEDGMENTS

This work was supported in part under the Cooperative Agreement between the Masdar Institute of Science and Technology, Abu Dhabi, UAE and the Massachusetts Institute of Technology, Cambridge, MA, USA, Reference Number 02/MI/MIT/CP/11/07633/GEN/G/00.

## REFERENCES

1. A. Fujishima and K. Honda. "TiO2 photoelectrochemistry and photocatalysis," Nature 238.5358, pp 37-38 1972.
2. K. Kashimoto, H. Irie and A. Fujishima, “TiO2 Photocatalysis: A Historical Overview and Future Prospects,” Japanese Journal of Applied Physics, vol. 44, no. 12, pp. 8269–8285, 2005.

3. D. Wang, Y. Liu, B. Yu, F. Zhou and W. Liu “TiO2 Nanotubes with Tunable Morphology, Diameter, and Length: Synthesis and Photo-Electrical/Catalytic Performance,” Chemical material *21* (7), pp. 1198–1206, 2009.
4. C. Clavero, “Plasmon-induced hot-electron generation at nanoparticle/metal-oxide interfaces for photovoltaic and photocatalytic devices,” Nature Photonics, vol. 8, no. 2, pp. 95-103, Feb. 2014.
5. J. B. Chou, D. P. Fenning, Y. Wang, M. A. M. Polanco, J. Hwang, F. Sammoura, J. Viegas, M. Rasras, A. Kolpak, Y. Shao-Horn and S.-G. Kim, “ Broadband Photoelectric Hot Carrier Collection with Wafer-Scale Metallic-Semiconductor Photonic Crystals,” 42nd IEEE PVSC Conference, New Orleans, LA, USA, June 2015
6. S. C. Warren and E. Thimsen, “Plasmonic solar water splitting,” Eenrgy & Environmental Science, vol. 5, no. 1, pp. 5133-5126, Jan. 2012.
7. http://rredc.nrel.gov/solar/spectra/am1.5/astmg173/astmg173.html, Nov. 2015.